

# Broad-tailed force distributions and velocity ordering in a heterogeneous membrane model for collective cell migration.

Tripti Bameta,<sup>1</sup> Dipjyoti Das,<sup>1</sup> Sumantra Sarkar,<sup>1</sup> Dibyendu Das,<sup>1,\*</sup> and Mandar M. Inamdar<sup>2,†</sup>

<sup>1</sup>*Department of Physics, Indian Institute of Technology, Bombay, Powai, Mumbai-400 076, India*

<sup>2</sup>*Department of Civil Engineering, Indian Institute of Technology, Bombay, Powai, Mumbai-400 076, India*

(Dated: June 14, 2018)

Correlated velocity patterns and associated large length-scale transmission of traction forces have been observed in collective live cell migration as a response to a “wound”. We argue that a simple physical model of a force-driven heterogeneous elastic membrane sliding over a viscous substrate can qualitatively explain a few experimentally observed facts: (i) the growth of velocity ordering which spreads from the wound boundary to the interior, (ii) the exponential tails of the traction force distributions, and (iii) the swirling pattern of velocities in the interior of the tissue.

PACS numbers: 87.18.Hf

## I. INTRODUCTION

The phenomenon of collective cell migration arises in biological processes of morphogenesis, wound healing, as well as cancer growth, and is an active topic of current research interest [1–7]. To understand the basic features in collective cell migration as a response to wound healing, two-dimensional monolayer patches of Madin-Darby canine kidney (MDCK) cells on deformable substrates have been studied in different experiments [4, 6–8].

For a physical scientist, there are many interesting aspects that these experiments reveal. The spatially heterogeneous swarming and swirling velocity patterns exhibited by the cells, studied by particle image velocimetry [6, 7], are reminiscent of similar pattern formation in active nematics and driven granular matter [9]. As time passes, a zone of velocity order starting from the wound boundary invades the interior of the MDCK tissue [7], reminding one of phase ordering kinetics [10]. On the other hand, another set of experiments [4, 8] have shown that the local traction forces exerted by the MDCK cells on the substrate have large fluctuations — the distribution of the forces being non-Gaussian with distinct broad exponential tails, akin to force distributions in static granular piles [11]. Yet, the MDCK cells forming the tissue are held to each other and to the substrate by a network of Cadherin and Integrin proteins, respectively [1, 12], and they self-generate active forces due to internal Actin and Myosin dynamics. Thus, at the microscopic level, they show no resemblance to mechanically driven loose granular rods or discs. Needless to say, it is quite a challenge to model every observed feature of the MDCK tissue system, as seen in different sets of experiments. In this paper, we propose a simple statistical–mechanical model for the system and show that it can simultaneously give a qualitative explanation of the growth of velocity ordering

with time, and the large force fluctuations.

It is well known that the behaviour of large cell collectives [14] is qualitatively distinct from that of a single cell [15]. Attempts have been made to model cell assemblies incorporating signal transduction and cell-cell signaling in *Dictyostelium discoideum* [16]. Collective cell migration studies incorporating cell division has been done [17–21], but the experiments that we are concerned with [4, 6, 7] have noted, that over the relevant time-scales, the growth of cell number via cell division is not expected to play a role in the features of interest in this paper. The geometrical instabilities such as fingering and tip-splitting of the wound boundary in experiments [6, 7] have been theoretically modelled using ideas of interface growth kinetics [2, 24]. The velocity patterns in the interior of the cell-sheet [6, 7] have recently been studied by a mechanical model, where the cells with a local orientation field collectively behave in a viscoelastic fashion [3]. We show below that a much simpler model compared to these can nevertheless capture two key features of the MDCK tissue system, namely, the velocity ordering invasion, and the large force fluctuations. In particular, the novel aspect of our model is to show the crucial role that heterogeneity plays in determining the large force fluctuations.

The paper is arranged in the following fashion. In section II we describe our model in details, and justify its various components on the basis of relevant experimental findings. We also specify the equations and the parameter values used for the simulation study of the model. In section IIIA–C we describe the three major findings of our model. Numerical estimates to make quantitative connections with the experiments are detailed in section III D. The significance of our model and findings in comparison with previous theoretical works are discussed in section IV.

\*Electronic address: dibyendu@phy.iitb.ac.in

†Electronic address: minamdar@civil.iitb.ac.in

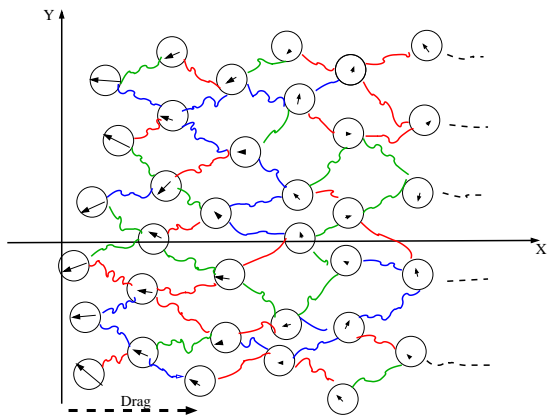


FIG. 1: A schematic picture (top view) of the deformed discretized membrane modeled as a tilted square lattice with undeformed spring-length  $a_0$  of unity. The wound boundary cells move towards  $-ve X$ . The cells are denoted by the circles and the active forces are denoted by arrows (size proportional the force magnitude) on them. The varying spring stiffnesses are denoted by multiple colors. The overall average substrate resistance is denoted by *Drag*.

## II. MODEL AND PARAMETERS

We model the cell sheet as an elastic membrane, although some earlier studies have treated cell monolayers as viscoelastic [3, 13]. The motivation for this choice comes from the experimental finding [7] that the average distance between MDCK cells does not change for many hours. It was clearly concluded that the movements of the cells are correlated showing very limited rearrangement, making the monolayer locally more elastic than viscous [7]. Similarly, a recent experimental study of internal stresses in cell monolayers [5] have also assumed the latter to be elastic. In our model, the cells are represented as discrete points in continuous space, and the cell-cell cadherin connections are represented by simple harmonic springs of effective stiffness  $\kappa_0$ . The elastic membrane is considered *heterogeneous* with  $\kappa_0$  drawn from a probability distribution function (p.d.f)  $P(\kappa_0)$ . Since there is inherent randomness in the number of intercellular cadherin connections [22], and the possibility of any such connection to be in multiple distinct structural states with different mechanical properties [23], our assumption of heterogeneity seems reasonable. Next, it is expected that the connections of the cells with the substrate via the integrin proteins will break and remake as the tissue advances [12]. For a single cell, it has been theoretically demonstrated that this complicated process of cell-substrate interaction can be effectively replaced by a *linear* viscous drag [25]. We extend the latter at the tissue level and assume that the substrate exerts a local drag force  $-c_0 \mathbf{V}_i$  where  $\mathbf{V}_i$  is velocity of the  $i$ -th cell and  $c_0$  is the drag constant. The average position of the “wound boundary” (see Fig. 1) defines the  $Y$ -direction, and the direction orthogonal to it will be called  $X$ . For

simulating, we take a  $N \times N$  tilted square grid of points (Fig. 1), but while thinking of a continuum limit, we will assume  $N \rightarrow \infty$  such that effectively the wound boundary will be very far from the center of the tissue (as in actual experiments [4, 7]). Finally, we supply the “live thrust forces” (originating from the cytoskeletal actomyosin activity in the cells) by hand in two alternate ways: (i) Cell- $i$  with position  $\mathbf{R}_i = (X_i, Y_i)$  is given a space and time dependent random force  $\mathbf{F}_i = \mathbf{F}_{ave,i} + \boldsymbol{\eta}_i$ , with  $\mathbf{F}_{ave,i} = -F_0 \exp(-n_i/\xi) \hat{\mathbf{x}}$ . Here  $n_i$  is the row number, from the boundary, of the  $i^{\text{th}}$  cell. The boundary row is numbered 0, and  $\xi$  is a length scale. The components of  $\boldsymbol{\eta}_i \equiv (\eta_X, \eta_Y)_i$  are Gaussian white noise with zero mean and  $\langle \eta_{\alpha,i}(t_1) \eta_{\beta,j}(t_2) \rangle = 2\sigma \exp(-n_i/\xi) \delta_{i,j} \delta_{\alpha,\beta} \delta(t_1 - t_2)$  with  $\alpha$  and  $\beta$  taking values  $X, Y$ . We will refer to this as participatory model (PM) (see Fig. 1). Thus in the PM model, the magnitude of the noise on force, just like the mean force, decays with increasing distance from the boundary. (ii) Only the cells at the wound boundary row are given a space and time dependent random force with an average force  $\mathbf{F}_{ave,i} = -F_0 \delta_{n_i,0} \hat{\mathbf{x}}$  added to Gaussian white noise  $\boldsymbol{\eta}_i$ , with zero mean and  $\langle \eta_{\alpha,i}(t_1) \eta_{\beta,j}(t_2) \rangle = 2\sigma \delta_{i,j} \delta_{\alpha,\beta} \delta(t_1 - t_2)$  ( $\alpha \equiv \{X, Y\}$ ,  $\beta \equiv \{X, Y\}$ ). We will refer to this as the leader driven model (LDM).

The motivation for comparing PM versus LDM comes from the discussions in Ref. [26] following the experiment of Ref. [4]. The mathematical equation used to simulate the system is:

$$c_0 \frac{d\mathbf{R}_i}{dt} = \sum_j \kappa_0^{ij} (|\mathbf{R}_j - \mathbf{R}_i| - a_0) \mathbf{e}_{ij} + \mathbf{F}_i. \quad (1)$$

The inertial term has been dropped as the system is clearly overdamped. The index  $j$  in the sum in Eq. 1 goes over nearest neighbours of  $i$  and  $\kappa_0^{ij}$  is the random stiffness constant of the spring connecting  $i$  and  $j$ . The unit vector  $\mathbf{e}_{ij} = (\mathbf{R}_j - \mathbf{R}_i)/|\mathbf{R}_j - \mathbf{R}_i|$ , and  $a_0$  is the undeformed length of the spring.

Here we report numerical results with parameter values:  $c_0 = 10$ ,  $N = 128$ ,  $F_0 = 1$ ,  $\sigma = 0.2$ ,  $a_0 = 1$ , and  $P(\kappa_0^{ij})$  is a uniform box distribution between 0.25 to 0.75. We will show later that these choices of parameters lead to reasonable correspondence to experiments. In the presence of the active applied force  $\mathbf{F}_i$ , we time-evolve the positions  $\mathbf{R}_i$  using Eq. 1, and obtain the velocities  $\mathbf{V}_i$  as  $d\mathbf{R}_i/dt$ . The simulation results for Figs. 2, 3, and 4, are obtained by providing the cells with zero initial velocities, and initial random displacements (from the equilibrium positions) with components uniformly distributed over  $[-\delta, \delta]$ . This may be expected to be a generic initial condition for the cell collective. Periodic boundary conditions are assumed along  $Y$ .

## III. RESULTS

In this section we present the three important results of our model.

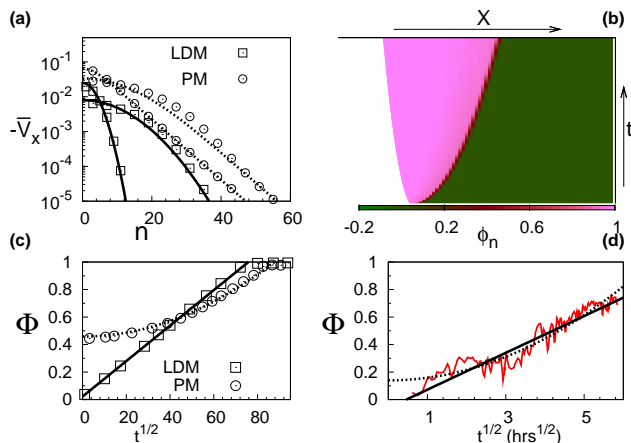


FIG. 2: Velocity ordering in the cell-sheet using  $\delta = 0.025$ . (a) Velocity of the cell points as a function of row number for two different times (100 and 1000). The circles and squares represent simulation results for PM ( $\xi = 5$ ) and LDM, respectively, and the fitting lines correspond to the theoretical model in Eq. 2. (b) The order parameter  $\phi_n$  at spatial position  $x$  of the cell at different times  $t$ . The  $x$ -range is 0 – 120 and  $t$ -range is 0 – 1000. The velocity ordering front is clearly visible. (c) The order parameter  $\Phi$  for the complete tissue, as a function of time  $t$ , with a fit of  $t^{1/2}$  and  $t$  for the LDM and PM, respectively. (d) Time dependence of experimental order parameter in [7] fitted with  $t$  and  $t^{1/2}$ .

### A. Invasion of Velocity Ordering

We first proceed to show how under the action of active forces the cell velocities acquire a bulk ordering. As the active forces are preferentially oriented along  $-\hat{x}$  (for both the LDM and PM), the velocities of the cells, starting with the ones close to the boundary and followed by the ones in the bulk, gradually orient themselves towards  $-\hat{x}$ . This velocity ordering is shown in Fig. 2(a) — with increasing time, for both the LDM and PM, mean row velocity  $-\overline{V}_X$  of deeper layers (with larger  $n$ ) rise in magnitude. Thus an order-disorder boundary moves towards larger  $n$ . Interestingly, there is a quantitative difference between the two models — the shape of the  $-\overline{V}_X(n)$  curve is Gaussian for LDM and has an exponential tail for PM. A local order parameter for every row  $n$  can be defined as  $\phi_n = -\overline{V}_{X,i}/|\overline{V}_i|$  (with all velocities  $-\overline{V}_{X,i} < 10^{-14}$  set to zero to avoid spurious contributions). In Fig. 2(b),  $\phi_n$  is plotted (with larger magnitude corresponding to lighter color) as a function of space  $X$  and time  $t$  for LDM — the movement of the order-disorder boundary with increasing  $t$  is clearly seen. A similar plot was observed experimentally in [7]. Next, a global order parameter for the whole system can be defined as  $\Phi = \langle \phi_n \rangle_n$ . In Fig. 2(c),  $\Phi$  is shown to increase as  $\sim t^{1/2}$  for LDM, and  $\sim t$  for PM. To compare with the experiments, we have plotted the experimental data for  $\Phi$  from [7] in Fig. 2(d); two curve-fits of  $\sim t^{1/2}$  and  $\sim t$  are put against the data, showing that both these

forms work reasonably well. Thus we have demonstrated numerically that our models have similar velocity ordering as seen experimentally in MDCK tissues [7] during wound healing. We will now proceed to understand analytically which ingredients of our model are essential for the above phenomenon, and in particular the reason for quantitative differences between LDM and PM.

It is interesting to note that the growth of  $V_X(t)$  above can be understood analytically from an analogous 1-dimensional problem. We can solve the one-dimensional problem of a pulled, non-disordered, elastic chain:

$$c_0 \frac{\partial u}{\partial t} = \kappa_0 \frac{\partial^2 u}{\partial x^2} + F(x, t). \quad (2)$$

The above equation is a simple 1-D, linearized, continuum version of Eq. 1. Here  $u(x, t)$  is the displacement of any cell,  $x \in [0, L]$  is the continuum space variable corresponding to the row number  $n_i$ , and the non-random force is  $F = -F_0 \exp(-x/\xi)$ , with  $\partial u/\partial x = 0|_{x=0}$  (for PM), and  $F = 0$ , with  $\partial u/\partial x = F_0/\kappa_0|_{x=0}$  (for LDM). The initial condition is taken as  $u(x, 0) = 0$  both for PM and LDM. Eq. 2 can be solved for velocity  $v(x, t) = \partial u/\partial t$  in the limit of large system size ( $L \rightarrow \infty$ ) with the boundary condition  $u(\infty, t) = 0$ . This gives unique analytical solutions:

$$\begin{aligned} \text{PM : } v(x, t) - v_{\text{CM}} &= -\frac{F_0}{2c_0} e^{(\tau - \tilde{x})} \left( 1 + \text{Erf} \left[ \frac{\tilde{x} - 2\tau}{2\sqrt{\tau}} \right] \right. \\ &\quad \left. + e^{2\tilde{x}} \text{Erfc} \left[ \frac{\tilde{x} + 2\tau}{2\sqrt{\tau}} \right] \right), \end{aligned} \quad (3)$$

$$\text{LDM : } v(x, t) - v_{\text{CM}} = -\frac{F_0}{\sqrt{c_0 \pi \kappa_0}} \frac{e^{-c_0 x^2 / 4 \kappa_0 t}}{\sqrt{t}}. \quad (4)$$

In Eq. 3 the symbols  $\tilde{x} = x/\xi$  and  $\tau = \kappa_0 t / c_0 \xi^2$  are scaled dimensionless space and time respectively, and Erf and Erfc refer to Error and Complementary Error functions [27], respectively. The profile of the ordered velocity as a function of  $x$  in the 1-D LDM model (Eq. 4) is clearly Gaussian, while in the PM model it is modified (Eq. 3) to have an exponential profile for large  $x$ . The agreement in mathematical forms between the 1-D analytical result and the 2-D simulation result in Fig. 2a shows that the velocity ordering phenomenon is not particularly dependent on stiffness randomness or noise, and its essence is captured even in a 1-D problem. As can be seen from Fig. 2c, the PM model gives a growth law  $\Phi \sim t$  for a transient period, the reason for which may be understood from Eq. 3. For large  $\tilde{x}$ ,  $\ln(-v(x)) \sim \tau - \tilde{x} + \text{Constant}$ , to leading order, while for small  $\tilde{x}$ ,  $\ln(-v(x)) \sim \tau - \tilde{x}^2 f(\tau) + \text{Constant}$  (see PM in Fig. 2a), where  $f(\tau)$  is a function of  $\tau$ . Thus there is a short distance quadratic profile, followed by a long distance linear profile in  $x$ . Spatial expanse of the quadratic profile keeps increasing, and beyond a certain time the growth law in PM will become  $\sim t^{1/2}$  just like LDM.

We would now like to see if a drive from the boundary cell layer without any participation from the cells in the bulk can invoke other experimentally observed phenomena. Hence, in the rest of the paper we focus on LDM.

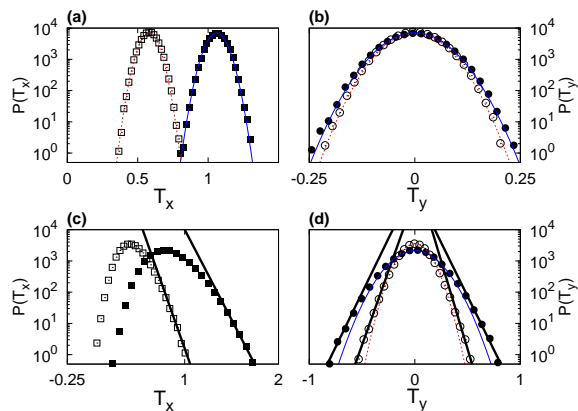


FIG. 3: Distributions  $P(\mathbf{T}_X)$  and  $P(\mathbf{T}_Y)$  of traction forces  $\mathbf{T}_X$  and  $\mathbf{T}_Y$  (in units of  $10^{-3}$ ) for LDM, at  $t = 300$  and  $\delta = 0.025$ . Gaussian fits are shown for uniform  $\kappa_0^{ij}$  in (a) and (b). For random  $\kappa_0^{ij}$ , deviation from Gaussianity, and resulting asymptotic exponential tails are shown in (c) and (d). The data is for layers 18 (filled symbols) and 19 (empty symbols).

### B. Traction Force Fluctuations

A second interesting result of our model is that the traction force fluctuations are unusually large as in the experiments in Ref. [4]. In our model, the local effective traction force on any cell is  $\mathbf{T}_i = \mathbf{F}_i - c_0 \mathbf{V}$  (see Eq. 1). In LDM,  $\mathbf{F}_i = 0$  (for any non-boundary cell) and so  $\mathbf{T}$ 's are proportional to the local velocities  $\mathbf{V}$ . The probability distributions of the components  $\mathbf{T}_X$  and  $\mathbf{T}_Y$  for the LDM are shown in Fig. 3. For homogeneous membrane (constant  $\kappa_0^{ij}$ ), the distributions are clearly Gaussian (Figs. 3(a-b)). To make sure that the latter is not a trivial consequence of the Gaussian distributed random thrust forces in the boundary layer, we checked the traction distributions when the boundary forces were drawn from a (i) box, and (ii) an exponential distribution. In both of these distinct cases, we found (data not shown) that the traction force components  $\mathbf{T}_X$  and  $\mathbf{T}_Y$  are Gaussian distributed. Thus there is no doubt that Central Limit Theorem (CLT) is valid and due to it, the local forces in the bulk (being sum of random neighbouring forces) turn out to be normally distributed. On the other hand, for a heterogeneous membrane (random  $\kappa_0^{ij}$ ) the distributions develop exponential tails (Figs. 3(c-d)), indicating a departure from the CLT. The shape of the curves of  $P(\mathbf{T}_X)$  (with mean at  $\mathbf{T}_X \neq 0$ ) and  $P(\mathbf{T}_Y)$  (with mean at  $\mathbf{T}_Y = 0$ ) have qualitative resemblance to experiments — in particular, the widths decrease with increase of distance from the wound.

Breakdown of CLT in [4] is *a priori* quite intriguing. It was speculated in Ref. [4], that a  $q$ -model [11] like mechanism maybe at play. Recognizing that the tissue is heterogeneous, here we are specifically suggesting that an effective  $q$ -model like mechanism may arise due to unequal stress propagation and accumulation mediated by

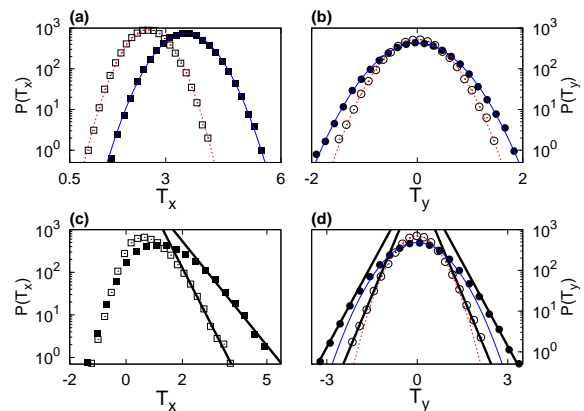


FIG. 4: Distributions  $P(\mathbf{T}_X)$  and  $P(\mathbf{T}_Y)$  of traction forces  $\mathbf{T}_X$  and  $\mathbf{T}_Y$  (in units of  $10^{-3}$ ) for LDM, at  $t = 300$ , for a distorted lattice with random bond lengths. The uniform stiffness constant  $k_0 = 1$ . Gaussian fits are shown for  $\epsilon = 0.15$  in (a) and (b). For  $\epsilon = 0.45$ , deviation from Gaussianity, and resulting asymptotic exponential tails are shown in (c) and (d). The data is for layers 18 (filled symbols) and 19 (empty symbols).

the random cadherin connections. Since the possibility of manipulating the strengths of cadherin connections has been experimentally demonstrated [5], our result is open to experimental test.

The membrane can also be made heterogeneous in another way by introducing variable bond lengths of the cell-cell connections, while keeping the spring stiffness homogeneous. This naturally leads to deviation from regular lattice symmetry considered so far. The bond lengths  $a_0^{ij}$  are made disordered by imparting new random equilibrium positions to the cells. To do so, the cells are shifted from the regular lattice by  $\epsilon_x$  (along-X) and  $\epsilon_y$  (along-Y), where  $\epsilon_x$  and  $\epsilon_y$  are drawn from uniform distribution over  $[-\epsilon, \epsilon]$ . As can be seen from Eq. 1, the magnitude and direction of the spring force is independent of the bond-length (to the first order). Thus for “small” lattice distortion the distributions for  $T_X$  and  $T_Y$  are expected to be the same as that of the uniform non-distorted lattice. This is seen in our simulations for a choice of  $\epsilon = 0.15$  —the traction distributions are indeed Gaussian (see Figs. 4(a) and 4(b)). Contrary to this, with “large” random lattice distortion, one would expect from Eq. 1 random harmonic forces, leading to a departure from the latter result. We indeed see this when we make  $\epsilon$  large (say 0.45) —the traction distributions develop exponential tails as shown in Figs. 4(c) and 4(d). Thus in two types of membrane heterogeneity —random spring stiffnesses and random bond lengths — we have found that non-Gaussian traction force distributions arise.

### C. Swirling Patterns in the Bulk

We now turn our attention to velocity patterns which develop in the bulk of the system. The cells in the con-

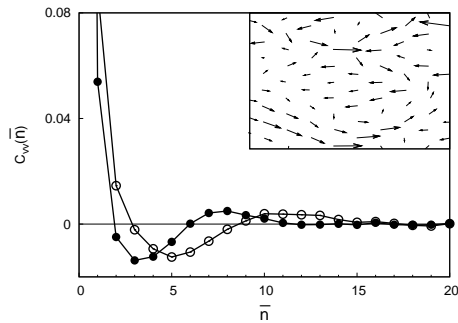


FIG. 5: The velocity-velocity correlation function  $C_{vv}$  against scaled distance  $\bar{n}$  along  $Y$ , at  $t = 500$  ( $\bullet$ ) and  $t = 1000$  ( $\circ$ ) for LDM using  $\delta = 0.45$ . Inset: Velocities of cells in the bulk region (dimension  $8 \times 8$ ) are shown (at  $t = 1000$ ) — swirls can be clearly seen.

finer region of the experimental setup in refs. [6, 7] are expected to be under internal stress due to the confinement from the boundary before the cell sheet is allowed to expand. In order to mimic this internal stress, we provide generic random initial positions to our cell lattice. The elastic relaxation of this “pre-strained” sheet help excite spatial modes through the harmonic couplings. The smaller wavelength modes damp out faster, leaving large wavelength velocity swirls at late times (inset of Fig. 5 for LDM). To precisely quantify the correlations in these patterns, we show the velocity-velocity correlation function  $C_{vv}(\bar{n}) = \langle \mathbf{v}(n_0) \cdot \mathbf{v}(n_0 + \bar{n}) \rangle / \langle \mathbf{v}^2 \rangle$  in Fig. 5; here  $\bar{n} = y/\sqrt{2}a_0$  is the scaled distance in units of average inter-cellular spacing along  $Y$ . The average  $\langle \dots \rangle$  is done over ensembles as well as cell locations  $n_0$ , belonging to a strip in the bulk region where  $\langle \mathbf{v}(n_0) \rangle = 0$ . We note that  $C_{vv}(\bar{n})$  shows change of sign beyond some layers (as seen also in experiments [28]) reflecting the bending of velocity field over space. The correlation range increases with the time of observation as expected — it is  $\approx 8 - 10$  cell layers which is roughly similar as distances seen in experiments [7, 28]. The correlations observed in ref. [28] are certainly influenced by substrate deformability and cell birth. But the fact that such correlations are also observed otherwise [6, 7] indicates that they may not be the only factors governing the swirling patterns. Although our model cannot make these distinctions we note that it elucidates the role of inherent elasticity and pre-strain of the cell-sheet in producing such patterns.

#### D. Numerical Estimates of Length, Time and Force Scales

We have shown so far that a boundary layer driven heterogeneous elastic sheet can produce qualitatively many experimental observations in collectively migrating epithelial cells. We now make numerical estimates of various quantities to find out whether our results are quantitatively meaningful in comparison with the experiments.

As shown in Fig. 1, the bond-length  $a_0$  is unity. In real units it may be taken as  $20\mu\text{m}$  (the average cell-cell separation [7]). To estimate the unit of time  $t_0$ , we start from Figs. 2(c) and (d). For the LDM in 2(c), the slope of the line in units of  $t_0^{-1/2}$  is 0.0139, while the experimental data in 2(d) has a slope  $0.139 \text{ hr}^{-1/2}$ . Equating the two, gives  $t_0 \approx 0.01\text{hr} = 36\text{s}$ . This tells us that the non-dimensional velocity in Fig. 2(a) in the boundary layer (for LDM)  $\sim 10^{-2}$  corresponds to  $10^{-2}a_0/t_0 \approx 20\mu\text{m}/\text{hr}$ . This is in the ball-park of the velocities quoted in experiments [7]. The curves in Fig. 2(a) are for times  $t = 1 \text{ hr}$  (100 in simulation) and 10 hrs (1000 in simulation). To make contact of forces in Fig. 3 with experiments, we choose to first obtain the bond-stiffness  $\kappa_0$  in real units. The properties of a continuum cell sheet may be chosen as those appearing in the supplementary material of [5]: Young’s modulus  $E = 10 \text{ kPa}$ , Poisson’s ratio  $\nu = 0.5$ , and sheet thickness of  $h = 5\mu\text{m}$ . We first consider a cell sheet of dimension  $a_0 \times a_0 \times h$ , on which homogeneous tension  $1 \text{ Pa}$  is applied. The relative change in surface area  $\Delta A/A = 2(1-\nu)/E = 10^{-4}$ . On the other hand, applying equivalent edge force of  $F = 1\text{Pa} \times a_0 \times h = 10^{-10} \text{ N}$  on a  $a_0 \times a_0$  square, whose sides are made of springs of stiffness  $\kappa_0$ , we get  $\Delta A/A = F/a_0\kappa_0$ . Equating the two relative area changes, we get  $\kappa_0 = 0.05 \text{ N/m}$ . But we have used an average stiffness value of 0.5 in dimensionless units in our simulation. This gives the actual force unit to be  $f_0 = 0.05 \times a_0/0.5 \text{ N} = 2 \times 10^{-6} \text{ N}$ . In dimensionless units our forces in Fig. 3 for the 19<sup>th</sup> layer are  $\sim 0.5 \times 10^{-3}$ , which is equivalent to  $10^{-9} \text{ N}$ . This implies a traction of  $10^{-9}/a_0^2 = 2.5 \text{ Pa}$ , which is one order of magnitude lower than that reported in [4]. The dimensionless time 300 reported in Fig. 3 translates to  $\approx 3 \text{ hrs}$ . Using  $a_0$ ,  $t_0$  and  $f_0$ , we see that the dimensionless value of  $c_0 = 10$  used in our simulation, is equivalent to  $10 \times f_0 t_0 / a_0 \approx 36 \text{ N-s/m}$  in real units. This can be converted into drag co-efficient  $\zeta = c_0/a_0^2 = 25 \text{ pN-hr}/\mu\text{m}^3$ , which is an order of magnitude lower than reported in [3]. In Fig. 5, at our simulation time  $t = 1000$  (equivalently  $\approx 10 \text{ hrs}$ ) the length scale associated with the first minimum of the correlation curve is  $5 \times a_0 = 100\mu\text{m}$ . In [28] at around 10 hrs, a similar reported length scale is  $200\mu\text{m}$  (or  $\approx 10$  cell layers), which is higher than our result only by a factor of two. Thus we see that, although our model is simple, it can make reasonably close contact to experiment even quantitatively.

One serious drawback is that our boundary tractions are very large  $\sim 10^3$  times compared to the bulk — in reality [4] forces do not diminish so fast. It would be interesting to modify LDM in the future by incorporating cellular thrusts from the bulk, to see if the description becomes more realistic in a quantitative sense.

## IV. DISCUSSION AND CONCLUSION

Recent experiments on collective migration of MDCK cells have thrown up several interesting puzzles, which in

turn have spurred various theoretical modeling attempts. Before we summarize the main results of this paper, we would like to situate our work with respect to the contributions made by the earlier theoretical models. The model of Ref. [3] treats the cell sheet as a viscoelastic medium supplemented with a director field to describe the local cellular orientations. This model obtains the dependence of the velocity of the wound boundary on the viscoelastic parameters of the cell-sheet, and also shows complex correlated velocity patterns in the bulk. Another model [2] concentrates specifically on the dynamics of the boundary of the cell-sheet. By introducing a competition between the curvature dependent driving force, and the elastic and viscous resistance of the cell sheet, the fingering instability as seen in experiment [7] is reproduced by this model. In contrast to these models, we treat the cell-sheet as an elastic membrane, and hope to capture some of the phenomena at early times. This is motivated by a direct experimental observation [7], and supported by treatment of cell-sheet as an elastic material in another set of experiments [5]. We note that the phenomena we address in this paper, namely, growth of bulk velocity order parameter [7], and traction force distributions [4] have not been addressed in the aforementioned publications [2, 3]. At the same time, the LDM cannot produce pronounced fingering due to the lack of *flowy* behaviour in our model. A very recent paper [20], which studies the effect of cell proliferation and migration leading to contact inhibition, introduces a simple one-dimensional model, where the cells *plastically* spread in presence of cellular thrust forces from the boundary (similar to LDM in our paper). Nevertheless, since this model is one-dimensional, quite naturally, it cannot capture the two-dimensional phenomenology.

In this paper we have identified few *minimal mechanical* ingredients — heterogeneous elastic membrane, fluid-

viscous drag, and the active drive of cells from the boundary to mechanically pull the system — which can explain three aspects of collective cell migration: (a) macroscopic velocity ordering, (b) breakdown of CLT for traction force fluctuations, and (c) velocity correlations associated with swirls. Perhaps the most interesting result is, that membrane heterogeneity has the capacity to induce broad tails in the distribution of traction forces. The mechanism that we propose here is very reminiscent of the q-model for static granular assemblies [11]. At the same time, we would like to point out that there are significant differences of our model from the q-model. We have a mobile network of cells, velocity dependent dissipative forces, and tensile force transmissions, as opposed to the static transmission of compressive forces in the granular assemblies. These differences may invite further analytical exploration of our current model in the future.

The three results in the paper show a close qualitative resemblance to the experiments. Even the quantitative estimates seem reasonable, albeit with a major drawback that the values of traction forces and velocities diminish much faster than the experimental values. This can be attributed to the fact that our model does not pump energy in the interior of the cell layer through active cellular thrusts. Recent experiments [5] hint that cellular polarizations and cellular active forces are possibly tied to mechanical stress cues from surrounding cells. This demands our model to go beyond being purely mechanical, by including a coupled dynamics (a cross-talk) between active cellular forces and mechanical harmonic forces. While we would explore these in future, we conclude by noting that this work sets a benchmark by showing the achievements and limitations of a rather simple mechanical model for collective cell migration.

- 
- [1] O. Llina and P. Friedl, *J. Cell Sc.* **122**, 3203 (2009).  
 [2] S. Mark *et al.*, *Biophys. J.* **98**, 361 (2010).  
 [3] P. Lee and C. Wolgemuth, *PLoS Comput. Bio.* **7**, e1002007 (2011); *Phys. Rev. E* **83**, 061920 (2011).  
 [4] X. Trepate *et al.*, *Nature Physics* **5**, 426 (2009).  
 [5] D.T. Tambe *et al.*, *Nature Materials* **10**, 469 (2011).  
 [6] M. Poujade *et al.*, *PNAS* **104**, 15988 (2007).  
 [7] L. Petitjean *et al.*, *Biophys. J.* **98**, 1790 (2010).  
 [8] O. du Roure *et al.*, *PNAS* **102**, 2390 (2005).  
 [9] J. Toner, Y. Tu and S. Ramaswamy, *Ann. Phys.* **318**, 170 (2005); V. Narayanan, S. Ramaswamy and N. Menon, *Science* **317**, 105 (2007); J. Deseigne, O. Dauchot, and H. Chaté, *Phys. Rev. Lett.* **105**, 098001 (2010).  
 [10] A. J. Bray, *Adv. Phys.* **43**, 357 (1994).  
 [11] C.-h. Liu *et al.*, *Science* **269**, 513 (1995); S.N. Copper-smith *et al.*, *Phys. Rev. E* **53**, 4673 (1996).  
 [12] B. Alberts *et al.*, *Molecular Biology of the Cell*, Garland Science (2008).  
 [13] J.D. Murray, *Mathematical Biology II: Spatial Models and Biomedical Applications*, Springer (2003).  
 [14] P. Rosen and D.S. Misfeldt, *PNAS* **77**, 4760 (1980).  
 [15] K. Larripa and A. Mogilner, *Physica A* **372**, 113 (2006); I. V. Dokukina and M. E. Gracheva, *Biophys. J.* **98**, 2794 (2010); V. S. Deshpande, R. M. McMeeking and A. G. Evans, *PNAS* **103**, 14015 (2006).  
 [16] E. Palsson and H.G. Othmer, *PNAS* **97**, 10448 (2000).  
 [17] M. Radszuweit *et al.*, *Phys. Rev. E* **79**, 051907 (2009).  
 [18] M.A. Stolarska, Y. Kim and H.G. Othmer, *Phil. Trans. R. Soc. A* **367**, 3525 (2009).  
 [19] J. C. Arcerio *et al.*, *Biophys. J.* **100**, 535 (2011).  
 [20] A. Puliafito *et al.*, *Proc. Nat. Acad. Sci. USA* **109**, 739 (2012).  
 [21] J. M. Osborne *et al.*, *Phil. Trans. R. Soc. A* **368**, 5013 (2010).  
 [22] T. M. Dobrowsky *et al.*, *Methods Cell Biol.* **89**, 411 (2008).  
 [23] S. Sivasankar, B. Gumbiner, and D. Leckband, *Biophys. J.* **80**, 1758 (2001).  
 [24] M.A.C. Huerigo *et al.*, *Phys. Rev. E* **82**, 031903 (2010).  
 [25] S. Walcott and S.X. Sun, *PNAS* **107**, 7757 (2010).

- [26] B. Ladoux, *Nature Physics* **5**, 377 (2009).
- [27] I.S. Gradshteyn and I.M. Ryzhik, *Tables of Integrals, Series and Products* (Academic Press, 2000).
- [28] T.E. Angelini *et. al.*, *Phys. Rev. Lett.* **104**, 168104 (2010).